JACS
JOURNAL OF THE AMERICAN CHEMICAL SOCIETY

Communication

pubs.acs.org/JACS

Interface Tension-Induced Synthesis of Monodispersed Mesoporous Carbon Hemispheres

Yin Fang,[†] Yingying Lv,[†] Feng Gong,[‡] Zhangxiong Wu,[§] Xiaomin Li,[†] Hongwei Zhu,[†] Lei Zhou,[†] Chi Yao,[†] Fan Zhang,[†] Gengfeng Zheng,[†] and Dongyuan Zhao*[,†]

[†]Department of Chemistry and Shanghai Key Lab of Molecular Catalysis and Innovative Materials, and Laboratory of Advanced Materials, Fudan University, Shanghai 200433, P. R. China

[‡]Department of Mechanical Engineering, National University of Singapore, Singapore 117576, Singapore

[§]Department of Chemical Engineering, Monash University, Wellington Road, Clayton, VIC 3800, Australia

Supporting Information

ABSTRACT: Here we report a novel interface tension-induced shrinkage approach to realize the synthesis of monodispersed asymmetrical mesoporous carbon nanohemispheres. We demonstrate that the products exhibit very uniform hemispherical morphology (130 × 60 nm) and are full of ordered mesopores, endowing them high surface areas and uniform pore sizes. These monodispersed mesoporous carbon hemispheres display excellent dispersibility in water for a long period without any aggregation. Moreover, a brand new feature of the mesoporous carbon materials has been observed for the first time: these monodispersed mesoporous carbon hemispheres show excellent thermal generation property under a NIR irradiation.

Symmetry and asymmetry are primary principles in nature.[1−3] Mesoporous materials have plenty of applications in catalysis,[4−7] energy storage and conversion,[8,9] separation, and biomedicine[10−17] due to their unique feature and properties. Ordered mesoporous materials have regular pore channels, high surface areas, and large pore volume,[4−6,18,19] which are considered as one feature of functional single-crystals (mesocrystals) due to their highly oriented mesostructures,[20−22] naturally exhibiting the primary principle of symmetry in mesophases. Thus, controlling or modifying their structures and morphologies to realize the asymmetry is still a great challenge.[23−27] Most of the reported mesoporous nanoparticles show regular spherical or rod-like morphologies. Anisotropic particles, such as patchy, misshapen, and Janus particles, have attracted significant attention in recent years due to their high complexity and are considered as a next-generation of building blocks for advanced materials and functional devices.[1,2] However, the controllable synthesis of the monodispersed asymmetrical mesoporous carbon nanoparticles has not been reported yet based on our best knowledge. The monodispersed mesoporous structures can integrate the advantages that are originated from mesopores (high surface area and large pore volume), nanoparticles (nanosized effects) into a single entity, showing novel properties and unique applications.[22,28,29] Moreover, discrete and dispersible mesoporous carbon nanoparticles are of critical importance for both the fundamental study and various practical applications such as drug delivery, catalysis, and so on.[30−32] However, all carbon nanostructures tend to condense and aggregate during the high-temperature annealing process. It remains a great challenge to produce mesoporous carbon nanoparticles with monodispersity and discreteness. In another aspect, core−shell nanostructures have captivated many attentions owing to their elegant structures with tunable functionality. Most current efforts in the core−shell structures are directed to developing new synthetic approaches with different components and shell structures. The interface interaction between core and shell is always ignored by researchers. However, the interface intension may be a positive route for the control preparation of unique nanostructures.

In this work, we demonstrate a novel synthesis approach: an interface tension-induced shrinkage on core−shell nanostructures interfaces to fabricate monodispersed asymmetrical mesoporous carbon nanohemispheres. Monodispersed mesoporous resin polymer nanospheres were used as a carbon source, and the core−shell structured polymer@SiO_2 spheres were obtained after coating a layer of amorphous silica on the surface, which created a closed spherical polymer−silica interface. The products exhibit very uniform anisotropic hemispherical morphology with a diameter of 130 nm and a height of 60 nm. These mesoporous carbon nanohemispheres have highly ordered mesopores, endowing them high surface areas and uniform pore sizes. Furthermore, as the protecting effect of the silica layer during the carbonization, these mesoporous carbon hemispheres are not aggregated and thus can be stably dispersed in solution for even a couple of months.

Moreover, the discovery of important roles of interface tension in the core−shell nanostructures may reveal a possible alternative to "classical" methods for the preparation of unique nanostructures. Furthermore, besides the well-known and widely applied features of mesoporous carbons (such as good conductivity or excellent adsorptivity), we have observed a brand new property here: these carbon hemispheres reveal excellent photothermal generation property for the mesoporous carbon for the first time; the temperature can be rapidly raised up to a very high temperature of 85 °C under a NIR irradiation in a few minutes. As a proof of concept, the findings provide an insight for building

Received: November 16, 2014
Published: February 13, 2015

DOI: 10.1021/jacs.5b01522
J. Am. Chem. Soc. 2015, 137, 2808−2811

a photothermal active platform by these mesoporous carbon hemispheres such as controlled release system and photothermal therapy agent.

SEM and TEM images show that the mesoporous carbon products are highly uniform with an asymmetrical hemispherical morphology (Figure 1). They seem to be cut at half off from

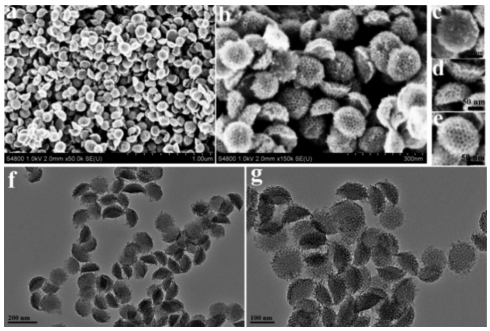

Figure 1. (a–e) SEM images of the mesoporous carbon hemispheres prepared by an interface tension-induced shrinkage. (c) Sectional faces, (d) side faces, and (e) spherical faces of the hemispheres. (f). Large-scale observation of the mesoporous carbon hemispheres. (g) Mesostructures of the hemispheres, observed from various directions: spherical face, sectional faces, and side faces.

intact nanospheres and have a radial diameter of 130 nm and a height of 60 nm. By HR-SEM images, ordered mesopores can be clearly observed on the surface of the nanohemispheres, and the pore size is estimated to be about 5–6 nm (Figure 1b–d). The ordered mesostructure is present across all hemispheres. Observed from the side, the hemispherical morphology can be further demonstrated. While the sectional face is not totally smooth, crescent protuberances can be found in the center, implying that the formation of the hemispheres is related with the interface-tension effect.

TEM images further confirm the hemispherical morphology of the monodispersed mesoporous nanoparticles, showing the uniform size (Figure 1f). The diameter of the hemispheres is ~130 nm, while the height is ~60 nm. The mesostructures of the carbon hemispheres are clearly demonstrated from observation in different locations (from the spherical faces, sectional and side faces) (Figure 1g). From the spherical and sectional faces of the hemispheres, mesopores with a diameter of 5–6 nm are arrayed in a close packing manner, implying a body-centered cubic symmetry of mesostructure. The mesopores are found to be distributed around the profile of hemispheres by close stacking, indicating the formation of the mesoporous hemispheres is related with the interface tension effect. SAXS patterns of the mesoporous carbon hemispheres show a broaden peak at q value of around 0.54 nm^{-1} (Figure S1). It is probably related with a small ordered domain size. The well-ordered mesostructure and high surface area (~770 $m^2 \cdot g^{-1}$) is further confirmed by the N_2 sorption isotherms (see more detail in Figure S2).

The formation process of the mesoporous carbon hemispheres is initialized from monodispersed polymer nanospheres. Through a sol–gel process, mesoporous polymer nanospheres are coated with a layer of amorphous silica (experimental section in the Supporting Information). TEM images of the as-made core–shell polymers@SiO_2 samples show that the mesoporous polymer spheres are closely attached with the silica layers (Figure 2a). After a carefully controlled drying procedure at room temperature, the polymer nanospheres are partially contracted.

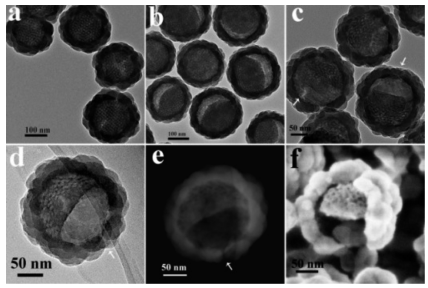

Figure 2. TEM images of (a) the as-made mesoporous resin polymers coated with a silica layer, creating a polymer–silica interface; (b) the samples after drying, 1/6 large cavity of the nanospheres is displayed; (c) the samples after calcination at 600 °C, half cavity of the nanospheres is discovered. (d) HR-TEM, (e) STEM, and (f) HRSEM images of the mesoporous carbon hemispheres coated with a layer of amorphous silica. The white arrows indicate the air vents on the silica shells.

About 1/6 volume of the cavity is exposed due to the volume contraction. It is interesting that the contraction is along the particular polar direction of the polymer cores (Figure 2b). After carbonization at 600 °C in N_2, the cavity is enlarged to 1/2 volume of the nanospheres, implying further volume contraction of the inner cores to carbon nanospheres (Figure 2c). Then, the core–shell hemisphere@cavity@silica nanostructure is formed. The mesopores on the hemispheres can be clearly observed (Figure 2d), demonstrating that the hemispheres are fully composed of ordered mesostructures. The hemisphere@cavity@silica nanostructures can further be confirmed by STEM (Figure 2e) and HR-SEM images of the cracked parts of the nanospheres (Figure 2f). By employing the initial polymer nanospheres with different particle sizes, the mesoporous carbon hemispheres with a variable diameter of ~135, 160, and 200 nm, respectively, can be obtained (Figure S3a–c). These nanostructures exhibit similar hemisphere@cavity@silica core–shell morphology; while the height of these hemispheres increases from 60 to 70 nm and finally to ~90 nm.

A high-temperature process can lead to further condensation and carbonization of the phenolic resin polymer spheres. With the temperature rising, the shrinkage of the mesoporous polymer spheres is aggravated, while the cavity is enlarged (Figure 3). We define R_c (red bar) to be the height of the cavity, and R_s (blue bar) as the height of the solid; and the ratio of R_c and ($R_s + R_c$) implies the shrinkage extent (Figure 3a–c). For the samples dried at 100 °C, the shrinkage extent along radius direction is measured to be ~13%. While with the temperature increasing, the shrinkage increases to ~35% at 350 °C and ~56% at 600 °C. These results indicate that the constriction of the polymer spheres and the height of the hemispheres are greatly affected by temperatures.

The polymer–silica interface plays an important role on the formation of hemispherical morphology (Figure 3d–i). For comparison, the case with absent polymer–silica interface was also examined. A selected etching method was employed to selectively remove the silica in a weak base solution (Na_2CO_3) and to form a yolk–shell nanostructures. When the polymer–silica interfaces are absent and the mesoporous polymer nanospheres are directly carbonized in N_2 atmosphere, uniform spherical mesoporous carbons instead of the hemispheres are obtained. After carbonization at 600 °C, the particle size is reduced from ~130 to 100 nm. Thus, the volume shrinkage of the polymer nanospheres is calculated to be ~54%. For the hemispheres prepared by the controlled interface-tension-induced shrinkage method, the whole volume shrinkage is

DOI: 10.1021/jacs.5b01522
J. Am. Chem. Soc. 2015, 137, 2808–2811

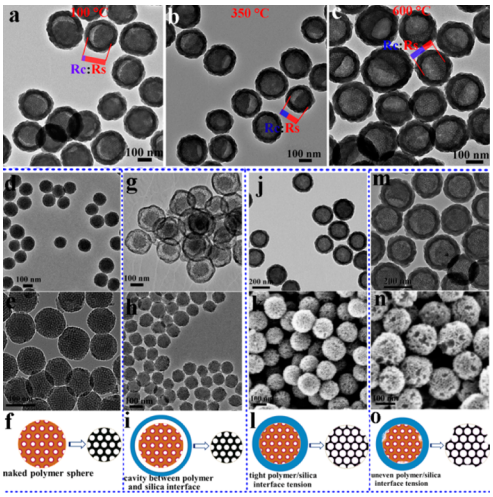

Figure 3. TEM images of the mesoporous carbon hemispheres with different shrinkage extent after calcined at temperatures of (a) 100; (b) 350; (c) 600 °C; R_c (red bar) means radius of the cavity, and R_s (blue bar) is the radius of the solid. TEM images of (d) the naked polymer nanospheres without silica layer and (e) the mesoporous carbon nanospheres derived from the polymer spheres; TEM images of (g) the polymer nanospheres with an unattached layer of silica and (h) the mesoporous carbon nanospheres after etching off the silica layer. (j) TEM and (k) HR-SEM images of the samples dried in a frozen drier, showing that the nanospheres keep spherical shapes. (m) TEM and (n) HR-SEM images of the samples dried at 100 °C in an oven, showing the partially cracked morphology.

measured to be ∼59%, agreeing well with that without silica layer coating.

Furthermore, the drying process also plays a key role in the formation process. The hemispheres can be fabricated under a mild room-temperature drying condition. It is interesting to note that some air vents on the silica shells are discovered on the cavity parts of the nanospheres (as shown by the arrows in Figure 2), implying that the formation process is probably related to the evaporated solvent steam. To further confirm this hypothesis, the room-temperature drying procedure is replaced with a frozen drying or/and a high temperature drying. Under the frozen drying procedure, the steam is frozen and reduced through this treatment (Figures 3j−l and S4). The condensed core−shell structures instead of the hemisphere@cavity@silica are formed after calcination. After etching off the silica shells, the nanospheres show integrated spherical morphology and accessible mesopores, instead of hemispherical morphology. Under the high temperature drying condition, as the steam is quickly evaporated, uneven shaped nanospheres are fabricated (Figure 3m−o). A partial cavity is found on each core−shell nanosphere, implying the uneven contraction during the high-temperature drying.

The formation of the ordered mesoporous carbon hemispheres has undergone an interface tension-induced shrinkage procedure (Scheme 1). The polymer−silica interface is introduced by in situ growth of a layer of amorphous silica on the surface of polymer nanospheres. During the synthesis, some Si−O−C chemical bonds are formed on the silica−polymer interface. The interface tension force tends to pull the polymer nanospheres close to silica shells (yellow arrows). In addition, the shrinkage of the polymer nanospheres occurs during the drying process, with a constriction tendency away from silica shells (green arrows). As all of the reactions are carried out in solution

Scheme 1. Formation Process of the Mesoporous Carbon Nanohemispheres through an Interface Tension-Induced Shrinkage

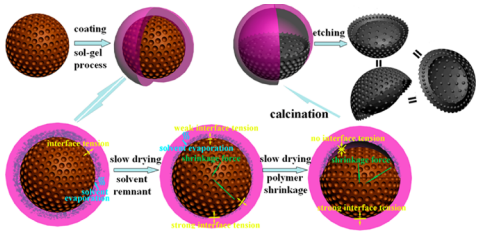

to keep the humidity of the whole system, parts of solvents originating from the sol−gel process remain inside the silica shells, and they evaporate and become steam during drying (blue arrows). This steam can insert and break the Si−O−C interconnections, leading to the reduction of the interface tension force. The steam repel, interface tension, and constriction force coexist and interact with each other at the same time during the process. Under the effect of constriction force, the polymer nanospheres shrink and constrict, thus the contraction is along particular polar direction because of the solvent steam repel force while retaining the spherical shape as the silica shell connection. Then asymmetrical nanostructures are constructed inside the silica shell. Finally, during the carbonization, the shrinkage degree is enlarged (∼50%) to form the hemispherical mesoporous carbon nanoparticles.

Through the controlled interface tension-induced synthesis strategy, the particular mesoporous carbon hemispheres can be fabricated. Meanwhile, the obtained carbon hemispheres display excellent dispersibility in water because with the silica layer coating[30,31] no aggregation between the carbon spheres occurred during the carbonization process. Even after 6 months' quiescence, the mesoporous carbon hemispheres are still dispersed well in water to form a uniform sol (Figure S5). The complete etching of silica layer is confirmed by TGA analysis of these carbon nanohemispheres (Figure S6). In comparison, the mesoporous carbon nanospheres prepared without the silica protector deposits on the bottom of water within 1 month.

The uniform and monodispersed mesoporous carbon hemispheres exhibit an excellent heat generation property under the near-IR (NIR) irradiation (Figure 4) because of nonaggregation. At a low concentration of the carbon hemispheres (50 μg/mL), rapid photothermal heating occurs upon irradiation by a low

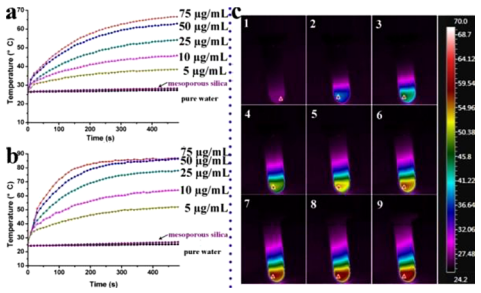

Figure 4. (a,b) Time-dependent photothermal activities of the mesoporous silica nanoparticles (25 μg/mL) and mesoporous carbon hemispheres with different concentrations in solution (labeled on graph) irradiated with 1 and 2 W/cm^2 laser. (c) Thermal images of the mesoporous carbon hemispheres with a concentration of 50 μg/mL irradiated with 808 nm laser at 1 W/cm^2 for (c1) 0; (c2) 1; (c3) 2; (c4) 3; (c5) 4; (c6) 5; (c7) 6; (c8) 7; and (c9) 8 min.

DOI: 10.1021/jacs.5b01522
J. Am. Chem. Soc. 2015, 137, 2808−2811

power laser (808 nm) at 1 W/cm^2 (Figure 4a). At every minute's interval, the color temperature of the hemispheres changes from cool color to warm color in the thermal images (Figure 4c). Samples irradiated by a laser with the higher energy density (2 W/cm^2) show superior photothermal heating (Figure 4b) than that with the lower one (1 W/cm^2) at all concentrations. Furthermore, the mesoporous carbon hemispheres exhibit a concentration-dependent photothermal heating effect (from 5 to 75 μg/mL), which increases monotonically with the hemisphere concentration. For the carbon hemispheres with a high concentration of 75 μg/mL, the temperature can raise up to 85 °C in a short time irradiation of 4 min (Figure 4b and Supplementary Movie S1), which is almost the highest temperature ever as far as we know. An off-lattice Monte Carlo method was built to simulate carbon nanohemisphere solutions under the illumination of near-infrared radiation (shown in Supporting Information). In this simulation, we build up the models by consideration of the morphology, size, and concentration of the nanohemispheres. Our simulation results obtain good agreement with the experimental data. The heat generation process can be understood by lack of sp^2 carbon atoms in the amorphous mesoporous carbon hemispheres, in which almost all of the light energy adsorbed is transferred into heat (Figure S7). In contrast, for the mesoporous silica nanoparticles, no obvious temperature raise is observed (Figure 4), suggesting the poor photothermal effect. However similar to silica materials, the mesoporous carbon nanoparticles are demonstrated to be good drug nanocarriers.[24,29] Thus, these carbon hemispheres may possess benefits in building photothermal response platform. As a proof of concept, a controlled release system and photothermal therapy based on the mesoporous carbon hemispheres have been established and tested (Figures S8 and S9).

In conclusion, monodispersed asymmetrical mesoporous carbon nanohemispheres with a diameter up to ∼130 nm and a height of ∼60 nm have been successfully fabricated by a controlled interface tension-induced shrinkage synthesis approach for the first time. Meanwhile, these uniform hemispheres have a well-ordered mesostructure, a high surface area (∼770 m^2·g^{-1}), and a large pore volume (∼1.0 cm^3·g^{-1}) and can be discrete and well dispersed in water for a long period without any aggregation. Moreover, these monodispersed carbon hemispheres show excellent thermal generation property under a NIR irradiation, revealing the photothermal generation property of the mesoporous carbon materials for the first time. As a proof of concept, these mesoporous carbon hemispheres may possess benefits in building photothermal response platform such as controlled release system and photothermal therapy agent.

■ ASSOCIATED CONTENT

Supporting Information

Experimental details, additional figures, and supplementary movie. This material is available free of charge via the Internet at http://pubs.acs.org.

■ AUTHOR INFORMATION

Corresponding Author

*dyzhao@fudan.edu.cn

Notes

The authors declare no competing financial interest.

■ ACKNOWLEDGMENTS

The work was supported by the Key Basic Research Program (2013CB934104, 2012CB224805), the NSFC (21210004, 21322311), and Shanghai Foundation of S&T Project (14JC1400700).

■ REFERENCES

(1) Walther, A.; Muller, A. H. *Chem. Rev.* **2013**, *113*, 5194.
(2) Hu, J.; Zhou, S.; Sun, Y.; Fang, X.; Wu, L. *Chem. Soc. Rev.* **2012**, *41*, 4356.
(3) Petkovich, N. D.; Stein, A. *Chem. Soc. Rev.* **2013**, *42*, 3721.
(4) Wan, Y.; Zhao, D. *Chem. Rev.* **2007**, *107*, 2821.
(5) Davis, M. E. *Nature* **2002**, *417*, 813.
(6) Tang, J.; Liu, J.; Torad, N. L.; Kimura, T.; Yamauchi, Y. *Nano Today* **2014**, *9*, 305.
(7) Lu, A. H.; Nitz, J. J.; Comotti, M.; Weidenthaler, C.; Schlichte, K.; Lehmann, C. W.; Terasaki, O.; Schuth, F. *J. Am. Chem. Soc.* **2010**, *132*, 14152.
(8) Ma, T. Y.; Liu, L.; Yuan, Z. Y. *Chem. Soc. Rev.* **2013**, *42*, 3977.
(9) Zhai, Y.; Dou, Y.; Zhao, D.; Fulvio, P. F.; Mayes, R. T.; Dai, S. *Adv. Mater.* **2011**, *23*, 4828.
(10) Chen, Y.; Chen, H. R.; Shi, J. L. *Acc. Chem. Res.* **2014**, *47*, 125.
(11) Li, Z.; Barnes, J. C.; Bosoy, A.; Stoddart, J. F.; Zink, J. I. *Chem. Soc. Rev.* **2012**, *41*, 2590.
(12) Chang, Y. T.; Liao, P. Y.; Sheu, H. S.; Tseng, Y. J.; Cheng, F. Y.; Yeh, C. S. *Adv. Mater.* **2012**, *24*, 3309.
(13) Wang, Y.; Wang, K. Y.; Zhao, J. F.; Liu, X. G.; Bu, J.; Yan, X. Y.; Huang, R. Q. *J. Am. Chem. Soc.* **2013**, *135*, 4799.
(14) Yang, J. P.; Shen, D. K.; Zhou, L.; Li, W.; Li, X. M.; Yao, C.; Wang, R.; El-Toni, A. M.; Zhang, F.; Zhao, D. Y. *Chem. Mater.* **2013**, *25*, 3030.
(15) Du, X.; Shi, B. Y.; Tang, Y. H.; Dai, S.; Qiao, S. Z. *Biomaterials* **2014**, *35*, 5580.
(16) Guillet-Nicolas, R.; Popat, A.; Bridot, J. L.; Monteith, G.; Qiao, S. Z.; Kleitz, F. *Angew. Chem., Int. Ed.* **2013**, *52*, 2318.
(17) Liu, R.; Zhang, Y.; Zhao, X.; Agarwal, A.; Mueller, L. J.; Feng, P. Y. *J. Am. Chem. Soc.* **2010**, *132*, 1500.
(18) Liang, C.; Li, Z.; Dai, S. *Angew. Chem., Int. Ed.* **2008**, *47*, 3696.
(19) Gu, D.; Schuth, F. *Chem. Soc. Rev.* **2014**, *43*, 313.
(20) Yu, C. Z.; Fan, J.; Tian, B. Z.; Zhao, D. Y. *Chem. Mater.* **2004**, *16*, 889.
(21) Gu, D.; Bongard, H.; Meng, Y.; Miyasaka, K.; Terasaki, O.; Zhang, F. Q.; Deng, Y. H.; Wu, Z. X.; Feng, D.; Fang, Y.; Tu, B.; Schuth, F.; Zhao, D. Y. *Chem. Mater.* **2010**, *22*, 4828.
(22) Fang, Y.; Gu, D.; Zou, Y.; Wu, Z. X.; Li, F. Y.; Che, R. C.; Deng, Y. H.; Tu, B.; Zhao, D. Y. *Angew. Chem., Int. Ed.* **2010**, *49*, 7987.
(23) Wu, Y.; Cheng, G.; Katsov, K.; Sides, S. W.; Wang, J.; Tang, J.; Fredrickson, G. H.; Moskovits, M.; Stucky, G. D. *Nat. Mater.* **2004**, *3*, 816.
(24) Lu, A. H.; Hao, G. P.; Sun, Q.; Zhang, X. Q.; Li, W. C. *Macromol. Chem. Phys.* **2012**, *213*, 1107.
(25) Valle-Vigon, P.; Sevilla, M.; Fuertes, A. B. *Chem. Mater.* **2010**, *22*, 2526.
(26) Suteewong, T.; Sai, H.; Hovden, R.; Muller, D.; Bradbury, M. S.; Gruner, S. M.; Wiesner, U. *Science* **2013**, *340*, 337.
(27) Li, F.; Yoo, W. C.; Beernink, M. B.; Stein, A. *J. Am. Chem. Soc.* **2009**, *131*, 18548.
(28) Liu, J.; Yang, T. Y.; Wang, D. W.; Lu, G. Q. M.; Zhao, D. Y.; Qiao, S. Z. *Nat. Commun.* **2013**, *4*, 2798.
(29) Fang, Y.; Zheng, G. F.; Yang, J. P.; Tang, H. S.; Zhang, Y. F.; Kong, B.; Lv, Y. Y.; Xu, C. J.; Asiri, A. M.; Zi, J.; Zhang, F.; Zhao, D. Y. *Angew. Chem., Int. Ed.* **2014**, *53*, 5366.
(30) Lu, A. H.; Hao, G. P.; Sun, Q. *Angew. Chem., Int. Ed.* **2013**, *52*, 7930.
(31) Wang, S.; Li, W. C.; Hao, G. P.; Hao, Y.; Sun, Q.; Zhang, X. Q.; Lu, A. H. *J. Am. Chem. Soc.* **2011**, *133*, 15304.
(32) Qiao, Z. A.; Guo, B. K.; Binder, A. J.; Chen, J. H.; Veith, G. M.; Dai, S. *Nano Lett.* **2013**, *13*, 207.

DOI: 10.1021/jacs.5b01522
J. Am. Chem. Soc. 2015, 137, 2808−2811